第 50 卷第 11 期 中国科学技术大学学报 Vol. 50, No. 11
2020 年 11 月 JOURNAL OF UNIVERSITY OF SCIENCE AND TECHNOLOGY OF CHINA Nov. 2020
Received：2020-11-08；Revised：2020-11-25 doi:10.3969/j.issn.0253-2778.2020.11.006

Structures，stabilities and spectra of endohedral mono-metallofullerenes M@C_{66}(M=Ca，Sr，Ba)：A first-principles study

CUI Peng[1, 2], ZHANG Zhuxia[3], Edward SHARMAN[4], JIANG Jun[2*]

1. *School of Information，Guizhou University of Finance and Economics，Guiyang* 550025，*China*；
2. *Department of Chemistry and Materials Science，University of Science and Technology of China，Hefei* 230026，*China*；
3. *College of Aeronautics and Astronautics，Taiyuan University of Technology，Taiyuan* 030024，*China*； 4. *Department of Neurology，University of California，Irvine，California* 92697，*USA*
*Corresponding author：jiangj1@ustc.edu.cn

Abstract：Structures of many endohedral metallofullerenes (EMF) are still unknown because of their very low production yield, especially for endohedral mono-metallofullerenes below C_{70}. In the present work, we investigated the alkaline earth metal encapsulated mono-metallofullerenes M@C_{66}(M=Ca, Sr, Ba) theoretically, compounds which have been detected only in mass spectra. The first-principles calculations and statistical thermodynamic analysis indicate that among the C_{66} isomers considered, the cage C_{2v}(4348)-C_{66} should be the most likely structure for M@C_{66}, M=Ca, Sr, Ba. These compounds may adopt another cage structure, C_2(4466)-C_{66}, at high temperatures. Both M@C_{2v}(4384)-C_{66} and M@C_2(4466)-C_{66} possess relatively large HOMO-LUMO gaps, and the former also possesses high local aromaticity. Thus it is predicted that M@C_{2v}(4348)-C_{66}—especially Ca@C_{2v}(4348)-C_{66}—could be isolable in future experiments. Moreover, simulated Vis-NIR, IR, Raman and ^{13}C NMR spectra are provided for assisting future experimental characterizations.

Keywords：metallofullerene; adjacent pentagon pairs; theoretical calculations
CLC number：O641 **Document code**：A

1 Introduction

Endohedral metallofullerenes (EMFs) attract more and more interest because of their unique structures, properties and applications in many fields such as photovoltaics, pharmaceuticals and quantum communications[1-3]. Many EMFs have been studied experimentally, in which one or several metal atoms or metal-containing clusters are encapsulated inside a fullerene carbon cage. Endohedral mono-metallofullerenes (EMMFs) are of special significance for exploring formation mechanisms of EMFs because of their simpler molecular structures, which facilities the understanding of the subtle interactions between metal and cage. Actually, the first experimentally isolated EMF was the EMMF La@C_{82} in 1991 [4]. Due to low production yields or solubility, determining the cage structure of EMFs is very difficult. For the alkaline earth metal-encapsulated EMMFs, as far as we know, only the structures of Ba@C_{74}[5] and Ca@C_{94}[6] have been determined directly by single crystal X-ray diffraction (XRD). Cage structures of some EMMFs have been determined indirectly using experimental tools such as Vis-NIR or ^{13}C NMR, but for most EMMFs, the cage structures are still totally unknown, even though many of these compounds have been detected by mass spectroscopy.

The isolated pentagon rule (IPR) is well-known for understanding the structures and stabilities of fullerene cages. Non-IPR fullerenes with adjacent pentagon pairs (APP) are unstable because the carbon at the bond shared by the fused pentagons (the [5, 5]-bond) is very pyramidal and labile; however such compounds can be stabilized by endohedral electron-donating metals or exohedral derivatization. Among the non-IPR fullerenes, C_{66}'s have attracted particular attention recently. Sc_2@C_{66} was one of the earliest reported EMFs with a non-IPR carbon cage [7], identified from the first as the C_{2v}(4348)-C_{66} isomer by NMR. Here C_{2v} is the symmetry of the empty cage, and 4348 is the Fowler-Manolopoulos number specified by the spiral algorithm. Which cage exists in the synthesized Sc_2@C_{66} was controversial for many years because according to theoretical calculations, another isomer—C_{2v}(4059)-C_{66}—is more stable when two Sc atoms are encapsulated [8, 9]. Recently, an XRD investigation has ascertained unambiguously that the Sc_2@C_{66} isomer is indeed the cage C_{2v}(4059)-C_{66}[10], a demonstration of the power and reliability of theoretical calculations. In the case of exohedral derivatization, XRD has identified two isomers of chlorofullerene, C_{2v}(4348)-C_{66} and C_s(4169)-C_{66}[11, 12].

Citation：CUI Peng, ZHANG Zhuxia, Edward SHARMAN, et al. Structures, stabilities and spectra of endohedral mono-metallofullerenes M@C_{66}(M=Ca, Sr, Ba): A first-principles study. J. Univ. Sci. Tech. China, 2020, 50(11): 1419-1430.

Recently, Tian et al. extracted a hydrofullerene $C_{66}H_4$ from combustion soot, for which the C_{66} cage possesses two APPs and two heptagons (termed "dihept-C_{66}")[13].

Li et al. investigated theoretically the C_{66}-based EMMFs in which the encapsulated atom is one of the rare earth metals Y, La, Tb and Yb [14]. They found the cage C_{2v} (4348)-C_{66} to be the predominant isomer adopted during the fullerene formation process. However, little is known of C_{66}-based EMMFs with one alkaline earth metal encapsulated, even though they have been observed previously in mass spectra [15]. It is interesting to know whether the structures of C_{66} cages encapsulating alkaline earth metals are different from those encapsulating rare earth metals, considering that alkaline earth metals possess two valence electrons whereas most rare earth metals possess three. Although previous calculations of C_{66} cage structures have shown that in the di-anion state the cage C_{2v} (4348)-C_{66} possesses the lowest energy, followed by the C_2(4466)-C_{66} and C_s(4169)-C_{66} isomers [16]; these calculations on a compound lacking encapsulated metals are insufficient to demonstrate the isomeric structure of alkaline-earth-encapsulated M@C_{66} cages (M = Ca, Sr, Ba). In fact, calculations on systems with explicit metal atom encapsulation are needed to produce a clear understanding. In addition, considering that a hydrogenated form of dihept-C_{66} with two heptagons has been discovered experimentally [13], are there any non-classical C_{66} isomers with heptagons among C_{66}-based EMMFs? In this work, by employing density functional theory calculations and statistical thermodynamic analysis, we investigated structures of the EMMFs M@C_{66}(M = Ca, Sr, Ba). The related electronic properties, kinetic stabilities and spectroscopic properties for the isomers most likely to be isolated in the future are predicted. As far as we know, this is the first report on the structures and properties of this class of compounds.

2 Computational details

There are 4478 classical isomers for fullerene C_{66} cages consisting of pentagons and hexagons, and none of them satisfies the IPR. When heptagons are involved, the number of possible isomers increases drastically. The number of C_{66} isomers with one heptagon is 132586 according to the spiral algorithm. In this work, isomers with no more than 5 APPs from the above mentioned 137064 isomers and the newly reported dihept-C_{66} isomer with two heptagons and two APPs [13] in their di-anion states were selected and allowed to relax computationally at the semi-empirical AM1 level. The isomers still in the di-anion state with relative AM1 energy below 40 kcal/mol were re-optimized at the density functional theory (DFT) level using the hybrid functional B3LYP and the basis set 6-31G(d). Next, isomers with relative B3LYP energies below 25 kcal/mol were chosen to be candidate cages for M@C_{66}(M = Ca, Sr, Ba). Geometry optimizations of M@C_{66} were carried out by employing both the hybrid functional B3LYP and the dispersion-corrected functional M062X. The latter functional was recommended recently for the computational structure elucidation of EMFs due to its inclusion of long-range corrections [17]. The Stuttgart/Dresdan (SDD) effective core potential and related valence basis set were selected for applying to Ca, Sr and Ba, in which Wood-Boring quasi-relativistic effects were considered. The standard 6-31G(d) basis set was selected for C atoms, and this combinational basis set is referred to as 6-31G* ~ SDD hereafter. Vibrational frequency calculations at the same level of theory as geometry optimization were performed to confirm that the obtained structures are true minima on the potential surfaces and could thus be used in the statistical thermodynamic analyses. Considering the high-temperatures required for production of EMFs, temperature-dependent molar fractions (x_i) of the i isomers of M@C_{66} were calculated with partition functions (q_i) and relative energies (ΔE_i) by the following expression

$$x_i(T) = \frac{q_i \exp[-\Delta E_i/(RT)]}{\sum_j q_j \exp[-\Delta E_j/(RT)]},$$

where T is the absolute temperature and R is the ideal gas constant. The partition functions were calculated using the rigid rotor and harmonic oscillator (RRHO) models, which have been widely used to study temperature-dependent concentrations of isomers of EMFs [14]. It should be noted that q_i for cages with chirality were doubled, taking into consideration the enantiomeric contribution.

The triplet-singlet splitting energies ($E_{T\text{-}S}$), vertical ionization energies (E_{VI}), adiabatic ionization energies (E_{AI}), vertical electron affinity energies (E_{VA}), and adiabatic electron affinity energies (E_{AA}) were calculated at the level of B3LYP/6-31G(d)~SDD. IR and Raman spectra were simulated at the same level of theory. ^{13}C NMR spectra and nucleus-independent chemical shifts (NICS) [18] were calculated using the gauge-independent atomic orbital (GIAO) method [19] with the functional B3LYP, and a larger basis set 6-311G* was selected for carbon atoms to describe the core electrons better. The NICS(1) index was also considered by calculating the chemical shift value at the point 1Å above the center of carbon ring outside the cage. Vis-NIR spectra were simulated using time-dependent density functional theory (TDDFT) with the functional BP86, which often performs better at simulating Vis-NIR spectra for EMFs [20]. Here, the diffuse function included basis set 6-31+G(d) was used for C atoms.

All calculations were performed using Gaussian 09 software[21]. The software CaGe [22] was used to generate

initial structures of C_{66} isomers, and the molecular graphics software VMD [23] was used to visualize molecular structures and molecular orbitals.

3 Results and discussion

3.1 Relative energies and thermodynamic stabilities of M@C_{66}

Based on the ionic model, carbon cages in M@C_{66} should be in their di-anion charge state, because the two valence electrons of the encapsulated alkaline earth metal can be formally donated to the outside cage. A total of 2800 isomers of C_{66} with no more than 5 APPs were optimized in their di-anion states at the AM1 level, and relative energies so obtained are plotted in Fig. S1. Clearly, the isomers with fewer APPs have lower energies, which demonstrates that the pentagon adjacency penalty rule (PARR) [24] still works well for the di-anion charge state. The 35 isomers with the lowest AM1 energies as well as the isomer C_{2v}(4059)-C_{66} existing in Sc2@C_{66} were re-optimized at the B3LYP/6-31G(d) level in their di-anion states. The relative energies so obtained and gaps between the highest occupied molecular orbital (HOMO) and the lowest unoccupied molecular orbital (LUMO) are listed in Tab. S1, as well as relative energies calculated at the AM1 level. One finds that the isomer C_{2v}(4348)-C_{66} has the lowest energy among the 35 di-anion isomers at both theory levels, which is also in line with previous calculations by Cui et al [16]. The 10 C_{66} isomers with relative B3LYP energies below 25.0 kcal/mol were considered to be candidate cages for M@C_{66}. The isomer dihept-C_{66} and C_{2v}(4059)-C_{66} were not considered further because their B3LYP energies are higher than that of C_{2v}(4348)-C_{66} by as much as 34.4 and 61.0 kcal/mol in the di-anion state, respectively.

Then the mono-metallofullerenes M@C_{66} with the 10 candidate cages were optimized using both B3LYP and M062X. The resulting relative energies (including zero point vibrational energies) and HOMO-LUMO gaps are listed in Tab.1. Cages of the 4 lowest-energy M@C_{66} isomers are the same as the 4 C_{66} cages with 2 APPs (see Fig. S1), independent of M being Ca, Sr or Ba. The EMMF isomer M@C_{2v}(4348)-C_{66} always has the lowest energy and the largest HOMO-LUMO gap, in accord with the di-anion C_{66} isomers. The second lowest-energy isomer is M@C_2(4466)-C_{66} with M being Sr or Ba, followed by the third lowest-energy isomers M@C_s(4169)-C_{66}, which is also consistent with the empty C_{66}^{2-}. In contrast, for Ca@C_{66}, the second lowest-energy isomer is Ca@C_s(4169)-C_{66}, which is lower by 2.1 kcal/mol than the third lowest-energy isomer Ca@C_2(4466)-C_{66} at the B3LYP level (3.7 kcal/mol for the M062X). This means that the ionic radius of the metal can change the energy order of EMMF isomers in some instances. The isomer M@C_1(*hep*28407)-C_{66} is the fourth lowest-energy isomer, and is the most stable M@C_{66} with a heptagon-containing C_{66} cage. Here we use *hep* to indicate the cage is heptagon-containing, and 28407 is the sequence number when the cage is generated by the CaGe software. This C_{66} cage C_1(*hep*28407)-C_{66} can be obtained in one step of the Stone-Wales transformation [25] from the classical C_{66} isomers C_2(4466)-C_{66}, Cs(4169)-C_{66} or C_1(4388)-C_{66}. The two functionals B3LYP and M062X give almost the same energy order for these 10 considered M@C_{66} isomers, which probably means that dispersion interaction is not very important for EMMFs. Moreover, single-point energy calculations using the larger 6-311G(d)～SDD basis set were performed, and the energy order obtained was unchanged, as can been seen in Tab.S2.

Tab. 1 Relative energies (ΔE, in kcal/mol, with zero point vibrational energy) and HOMO-LUMO gaps (Gap, in eV) of the 10 lowest energy isomers of M@C_{66}(M=Ca, Sr, Ba) calculated using either the B3LYP or M062X (values in parentheses) functionals with the 6-31G(d)～SDD basis set.

Cage Isomer	NAPP[a]	Ca@C_{66}		Sr@C_{66}		Ba@C_{66}	
		ΔE	Gap	ΔE	Gap	ΔE	Gap
C_{2v}(4348)	2	0.0 (0.0)	2.24 (3.72)	0.0 (0.0)	2.21 (3.67)	0.0 (0.0)	2.14 (3.58)
C_2(4466)	2	14.7 (15.6)	1.95 (3.39)	12.3 (12.5)	1.96 (3.39)	9.6 (9.4)	1.98 (3.37)
C_s(4169)	2	12.6 (11.9)	1.81 (3.26)	15.3 (15.1)	1.70 (3.12)	15.3 (16.0)	1.54 (2.93)
C_1(*hep*28407)	2	20.9 (22.9)	1.73 (3.23)	20.2 (22.1)	1.68 (3.16)	19.0 (20.8)	1.60 (3.06)
C_1(*hep*28418)	3	22.4 (25.7)	1.93 (3.39)	21.4 (24.3)	1.91 (3.36)	20.4 (22.8)	1.88 (3.33)
C_1(4369)	3	25.2 (27.6)	1.80 (3.18)	23.3 (24.9)	1.84 (3.22)	20.5 (21.0)	1.90 (3.27)
C_1(4434)	3	25.1 (27.4)	1.80 (3.25)	23.7 (25.6)	1.83 (3.27)	22.1 (23.4)	1.84 (3.26)
C_1(4007)	3	25.7 (27.3)	1.66 (3.00)	27.0 (28.7)	1.60 (2.92)	25.3 (27.2)	1.54 (2.84)
C_1(*hep*28336)	3	28.7 (31.8)	1.53 (2.95)	28.7 (31.5)	1.57 (3.00)	25.8 (28.3)	1.66 (3.1)
C_1(4439)	3	29.9 (33.8)	1.37 (2.77)	28.7 (32.2)	1.39 (2.81)	26.7 (29.1)	1.44 (2.85)

[a] Number of adjacent pentagon pairs.

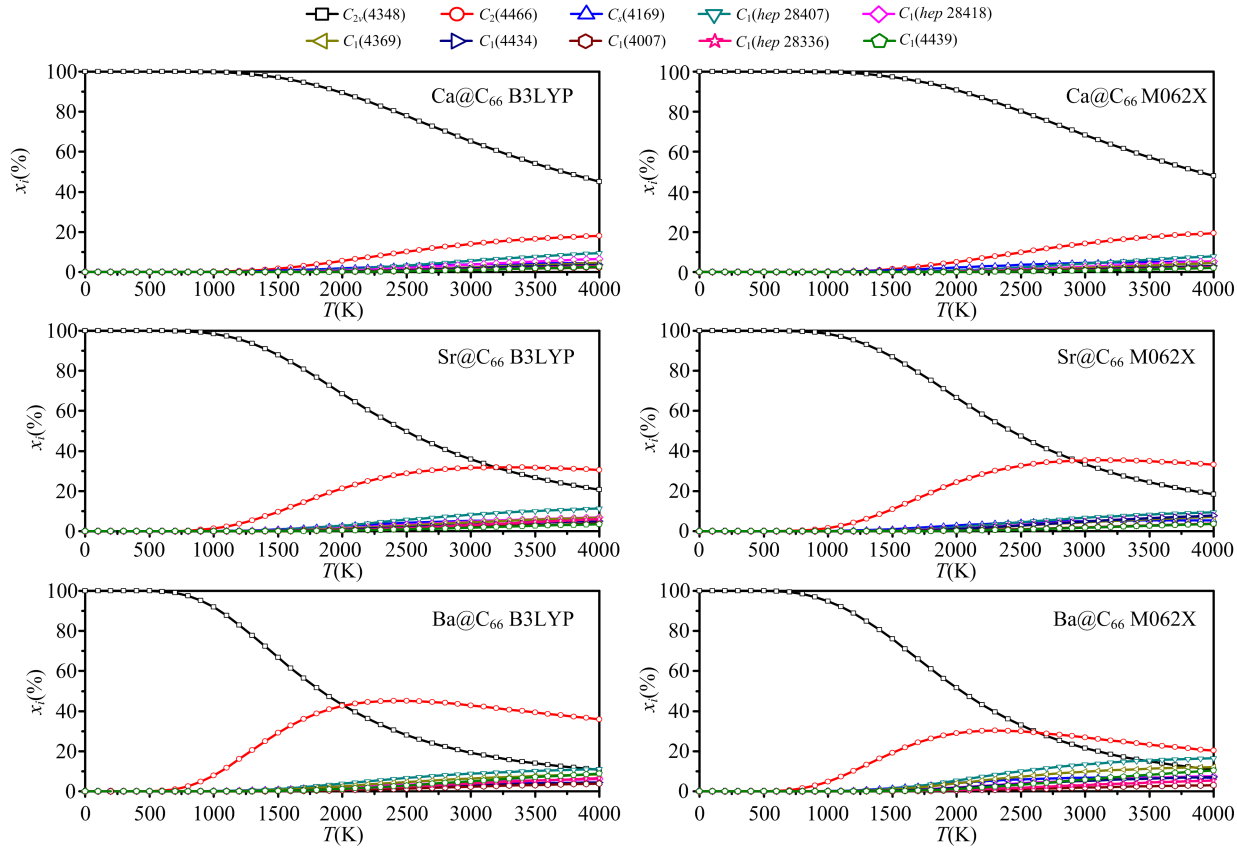

Fig. 1 Temperature-dependent concentrations of M@C_{66}(M=Ca, Sr or Ba) isomers calculated at B3LYP and M062X levels of theory.

Considering the standard arc-discharge conditions under which EMFs are typically synthesized, experimental production yields of EMF isomers are usually determined by their relative thermodynamic stabilities at high temperatures. Temperature-dependent molar concentrations of the10 isomers of M@C_{66}(M=Ca, Sr or Ba) over the temperature range 0 K～4000 K were calculated according to equilibrium statistical thermodynamics, at both the B3LYP and M062X levels of theory. As shown in Fig. 1, the molar concentration of the lowest-energy isomer M@C_{2v}(4348)-C_{66} decreases and that of the other 9 isomers rises with increasing temperature; among these isomers, the molar concentration of M@C_2(4466)-C_{66} increases most rapidly. This result is independent of M, indicating that the type of carbon cage plays a more decisive role in the production yield for EMMF. For Ca@C_{66}, the isomer Ca@C_{2v}(4348)-C_{66} predominates at all temperatures over the range from 0 K to 4000 K; despite the fact that its molar fraction decreases with increasing temperature, it still has the highest concentration (45.2% predicted by B3LYP and 48.0% by M062X) even at 4000 K. Aside from Ca@C_{2v}(4348)-C_{66}, the concentration of Ca@C_2(4466)-C_{66} becomes noticeably higher than the other 8 isomers when the temperature is above 2000 K; it is predicted to reach 18.4% by B3LYP and 19.4% by M062X at 4000 K. In comparison, the concentration of the second lowest-energy isomer Ca@C_s(4169)-C_{66} is predicted to be very low at all temperatures considered. For Sr@C_{66}, the mole fraction of the Sr@C_{2v}(4348)-C_{66} isomer is highest at low temperatures below 2500 K, while that of Sr@C_2(4466)-C_{66} increases rapidly, and is predicted to become the major isomer at temperatures above 3200 K at the B3LYP level and 3000 K at the M062X level, respectively. The two functionals B3LYP and M062X provided nearly the same results for Ca@C_{66} and Sr@C_{66}. The temperature-dependent concentrations of Ba@C_{66} isomers are rather similar to those of Sr@C_{66}, except that the concentration of the Ba@C_2(4466)-C_{66} isomer rises more rapidly, and exceeds that of Ba@C_{2v}(4348)-C_{66} at about 2100 K, becoming the dominant isomer at 4000 K (at the B3LYP level). Results calculated by M062X are a little different, in that concentrations of Ba@C_2(4466)-C_{66} and Ba@C_{2v}(4348)-C_{66} become equal at about 2600 K; however, both of them decrease at higher temperatures, and all 10 Ba@C_{66} isomers have comparable and low concentrations at 4000 K. This difference probably originates from the long-range dispersion interactions included in the M062X functional. Considering the very similar results of the two functionals M062X and B3LYP for Ca@C_{66} and Sr@C_{66}, it seems that dispersion interactions

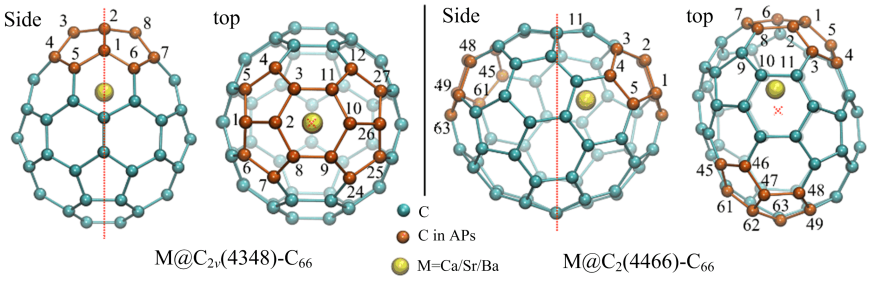

Fig. 2 Molecular structures of M@C_{2v}(4348)-C_{66}(M@**1**) and M@C_2(4466)-C_{66}(M@**2**) (M=Ca, Sr, Ba) from side and top perspectives. The APP motifs are highlighted in orange, and the C_2-axes are shown by red dot lines in the side views and red crosses in the top views.

contribute a noticeable effect only when the ionic radius of the encapsulated metal is large for EMMF, such as in the case of Ba investigated here.

Due to the fact that fullerene formation usually occurs at temperatures between 500 K and 3000 K, we can predict that the Ca@C_{66} isomer detected by mass spectrometry should be primarily Ca@C_{2v}(4348)-C_{66}, and M@C_{66} should be a mixture of M@C_{2v}(4348)-C_{66} and M@C_2(4466)-C_{66} for M=Sr or Ba. This conclusion is almost independent of the functional used, although M062X provides a somewhat different result at very high temperatures. As far as we know, this is the first time that cage structures of M@C_{66} with M being the alkaline metals Ca, Sr and Ba are determined, albeit theoretically.

3.2 Structures and kinetic stabilities of M@C_{2v}(4348)-C_{66} and M@C_2(4466)-C_{66}

According to the above analyses, C_{2v}(4348)-C_{66} and C_2(4466)-C_{66} should be the most probable cages existing in synthesized M@C_{66}(M=Ca, Sr, Ba). For the sake of simplicity, the two cages C_{2v}(4348)-C_{66} and C_2(4466)-C_{66} will be referred to hereafter as **1** and **2**, respectively. The optimized geometries are not very sensitive to the functional used. As can be seen in Tab.S3, the carbon atoms nearest to the encapsulated metal atom are all predicted to be the same by both B3LYP and M062X functionals. Hence, only the geometries optimized with B3LYP are discussed and used to calculate electronic properties and spectra.

The optimized geometries of M@**1** and M@**2** are displayed in Fig. 2 from two different perspectives. Both cages **1** and **2** have two APP motifs, which are colored orange. The two APPs in cage **1** are adjacent, and located at the same end of the C_2 axis. For cage **2**, the two APPs are also located at the same end of the C_2 axis, but the separation between them is larger, as can be seen in the top perspective of Fig. 2. In M@**1**, the metal atom is situated exactly along the C_2 axis of cage **1**, binds to the two adjacent APPs equally, and so the C_{2v} symmetry of the cage is maintained. The encapsulated metal in cage **2** is not situated along the C_2 axis, but asymmetrically binds with one of the two APPs, so the C_2 symmetry of cage **2** is broken, and hence there should be two equivalent sites for the metal in this cage. The difference in location of the metal in **1** and **2** mainly originates from the difference in separation between the two APP motifs. When the separation is small, such as in cage **1**, the encapsulated metal can coordinate with the two APPs equally, so most likely its location will be equidistant from them. When the separation is large, the encapsulated metal has to deviate from the center and approach one of the two APPs, otherwise it could coordinate with neither of them. On the other hand, the ionic radius of the encapsulated metal also plays an important role in its location in relation to the APPs. As can be found in Tab.S3, the metal moves farther away from its coordinating APP (C atoms belonging to the APP motifs can be read from Fig. 2) as its ionic radius increases from Ca to Sr to Ba for both M@**1** and M@**2**. But in M@**2**, M more nearly approaches the center between the two APPs as its ionic radius increases. For both M@**1** and M@**2**, the nearest carbon atom to the encapsulated metal is not always one of the [5, 5]-bonded carbons of the APP. For Ca@**1** and Sr@**1** the nearest carbon atom is C3 (and its equivalent atoms C8, C9 and C11), at distances of 2.51 Å and 2.76 Å, respectively, and for Ba@**1** the nearest carbon atom to Ba is C4 (and its equivalent atoms C7, C12 and C24), at a distance of 3.10 Å. For M@**2**, the shortest distance between M and carbon differs little from that in cage **1**, where the nearest carbon to Ca, Sr and Ba is C8, C9 and C11, with distances of 2.50 Å, 2.75 Å and 3.00 Å, respectively. Note that C9 and C11 of cage **2** do not actually belong to either of the two APPs, indicating it is not necessary that the nearest carbon to the encapsulated metal belong to an APP motif for non-IPR EMFs.

The kinetic stability of EMFs relates to their HOMO-LUMO gaps. Fullerenes and EMFs with small HOMO-LUMO gaps usually have low solubility in common organic solvents, and are thus hard to isolate by convention methods[26]. As shown in Tab. 1, HOMO-LUMO gaps for M@**1** and M@**2** calculated by B3LYP are in the range of 2.14 eV～2.24 eV and 1.95 eV～1.98 eV, respectively. For comparison, HOMO-LUMO gaps of

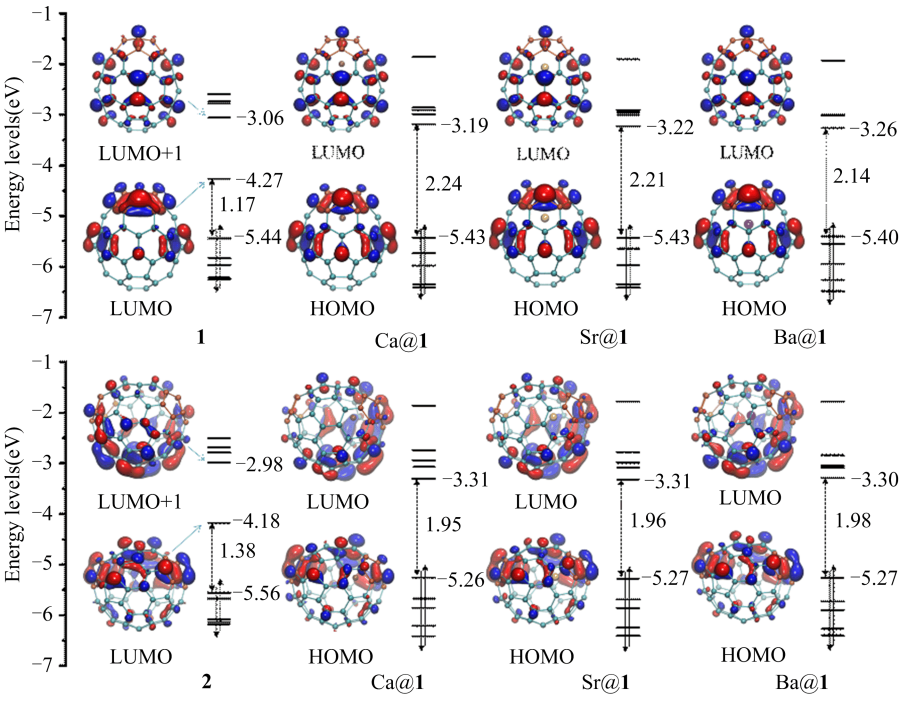

Fig. 3 Energy levels of main frontier molecular orbitals of pristine C_{2v}(4348)-C_{66}(**1**), pristine C_2(4466)-C_{66}(**2**), M@C_{2v}(4348)-C_{66}(M@**1**) and M@C_2(4466)-C_{66}(M@**2**) (M＝Ca, Sr, Ba). HOMOs and LUMOs are shown at isosurface value ±0.03.

the experimentally isolated M@C_{2v}(3)-C_{80}(M＝Ca, Sr, Ba) [27]. were calculated recently to be 1.61 eV～1.73 eV by B3LYP [28]. The gaps of another EMF M@C_1(17459)-C_{76}(M＝Ca, Sr, Ba) were reported to be 1.68 eV～1.71 eV calculated using the same functional [29]. These comparisons indicate that the HOMO-LUMO gaps of M@**1** and M@**2** investigated in this work are relatively large, and the resulting kinetic stability and good solubility in common organic solvents will facilitate their experimental isolation and characterization. The HOMO-LUMO gaps of M@**1** are always larger than those of M@**2**. As the ionic radius of M increases from Ca to Sr to Ba, the gap of M@**1** decreases from 2.24 eV to 2.14 eV, whereas the gap of M@**2** increases from 1.95 eV to 1.98 eV. It is interesting to note these very different trends. In cage **1**, the metal moves along the C_2 axis when we change the metal from Ca to Sr and to Ba. The distributions of HOMO and LUMO orbitals are also symmetric along the same axis. And the changes of energy for both HOMO and LUMO of M@**1** are obvious. The HOMO of M@**1** mainly distributes on the top and middle region of the cage, with a little more on the top region, as depicted in Fig. 3. Correspondingly, the HOMO energy increases a bit from Ca to Sr to Ba, as the metal is leaving the main part of its distribution. Similarly, LUMOs of those three M@**1** systems mainly distributes on the middle region of the cage. The LUMO energy decreases quite a bit from Ca to Sr to Ba. For M@**2**, the movement of the inside metal from Ca to Sr to Ba is not along the C_2 axis of the cage, so there are no significant changes for the HOMO and LUMO energies and HOMO-LUMO gap along with metal varying from Ca to Sr to Ba. Moreover, HOMO and LUMO of M@**1** and M@**2** are distributed almost completely on the outside of the cage, where the nature of M has little influence. The distribution of M@C_{66} HOMOs is nearly the same as those of LUMOs of empty cages **1** and **2**, meaning that both the two C_{66} cages can accept two electrons from the encapsulated metal, confirming the formal electronic structures M^{2+} @ C_{66}^{2-}. We have calculated the charges distributed on the encapsulated metal atom at the B3LYP level. The quantities of charges transferred between the M and C_{66} cages are 1.276 e, 1.301 e, 1.326 e for M@**1**, and 1.298 e, 1.331 e, 1.343 e for M@**2**, where M＝Ca, Sr, Ba, respectively. One can see that the charge transfer increases from Ca to Sr to Ba. For the same encapsulated metal, cage **2** seems to collect more negative charges from metal than cage **1**. LUMOs of M@**1** are very similar to LUMO＋1 of empty cage **1**, but LUMOs of M@**2** differ somewhat from the LUMO＋1 of empty cage **2**, which lean to the side of where M is located.

It is known that the APP motif of non-IPR fullerenes with 8π electrons violates Hückel's (4n＋2) rule and is highly antiaromatic[30]. Electrons transferred from an encapsulated metal can stabilize the APP according to the 'local-aromaticity' principle, and consequently many non-IPR fullerene cages have been synthesized and isolated in their EMF form [31]. Here we calculated

Tab. 2 NICS(0) (in ppm) and NICS(**1**) (values in parentheses, in ppm) of selected carbon rings of pristine C_{2v}(4348)-C_{66}(**1**), pristine C_2(4466)-C_{66}(**2**), M@C_{2v}(4348)-C_{66}(M@**1**) and M@C_2(4466)-C_{66}(M@**2**) (M=Ca, Sr, Ba).

Cage: Ring	C_{66}	Ca@C_{66}	Sr@C_{66}	Ba@C_{66}
1: Pentagon(C1-C2-C3)	18.1 (8.2)	−11.3 (−3.0)	−10.6 (−2.7)	−10.4 (−2.8)
1: Hexagon(C2-C3-C11)	20.4 (11.7)	−17.2 (−3.4)	−15.8 (−3.0)	−16.1 (−3.3)
2: Pentagon(C1-C2-C3)	12.0 (5.8)	−16.9 (−5.6)	−14.6 (−4.9)	−14.0 (−4.8)
2: Pentagon(C1-C2-C6)	11.8 (6.4)	−6.7 (−0.5)	−2.9 (0.8)	−1.7 (1.2)
2: Pentagon(C45-C46-C47)	12.0 (5.8)	−10.0 (−3.1)	−11.0 (−3.6)	−12.1 (−4.1)
2: Pentagon(C47-C48-C49)	11.8 (6.4)	−1.8 (1.3)	−1.9 (1.2)	−2.1 (1.1)

NICS at the center of and at a point 1Å above the pentagon rings of the APP motifs of the two C_{66} cages under study, where the former are referred to as NICS(0) and the latter as NICS(1). In addition, NICS for the hexagonal ring Hexagon(C2-C3-C11) between the two adjacent APPs of cage **1** were also calculated. The values obtained are listed in Tab.2. Note that negative NICS values indicate aromaticity and positive values indicate antiaromaticity. For empty C_{66} cages **1** and **2**, NICS(0) values of all the rings considered are positive and large, indicating they are highly antiaromatic. For M@**1** and M@**2**, all the NICS(0) values become negative, indicating that the encapsulated M indeed confers local aromaticity to the two non-IPR C_{66} cages **1** and **2**. The most significant change is to the ring Hexagon(C2-C3-C11) between the two APPs of cage **1**, the NICS(0) of which changing from 20.4 ppm for the empty cage to -17.2 ppm for Ca@**1**. The four equivalent pentagon rings with APP motifs in cage **1** also become highly aromatic after M is encapsulated. These results indicate that all three M@**1** have high local aromaticity. Among them, Ca@**1** is the most aromatic, with NICS(0) values of the two kinds of rings investigated being -17.2 ppm and -11.3 ppm, respectively. The values of NICS(1) of M@**1** also support this conclusion. The high local aromaticity of M@**1** makes them promising compounds to be isolated and characterized in future experiments, especially Ca@**1**. It should be pointed out that for most non-IPR EMFs and all the EMMFs synthesized up to now, a single encapsulated metal stabilizes only a single APP. The case of M@**1** is very special because one metal stabilizes two APPs at the same time. The local aromaticity of M@**2** induced by the encapsulated metal is not as great as that of M@**1**. For each of the two APPs, only one pentagon ring has high aromaticity. Of the two aromatic rings, the one closer to M has more negative NICS values. The other two pentagon rings of M@**2**, Pentagon (C1-C2-C6) and Pentagon (C47-C48-C49), have negative but small NICS(0) values and even smaller positive NICS(1) values, indicating that the two rings possess weak or no aromaticity. These would probably render the synthesis and isolation of M@**2** compounds difficult.

Tab. 3 Triplet-singlet splitting energies ($E_{T\text{-}S}$), vertical ionization energies (E_{VI}), adiabatic ionization energies (E_{AI}), vertical electron affinity energies (E_{VA}) and adiabatic electron affinity energies (E_{AA}) (all in eV) of M@C_{2v}(4348)-C_{66}(M@**1**) and M@C_2(4466)-C_{66}(M@**2**) (M=Ca, Sr, Ba).

M@C_{66}	$E_{T\text{-}S}$	E_{VI}	E_{AI}	E_{VA}	E_{AA}
Ca@**1**	1.49	6.60	6.54	2.01	2.07
Sr@**1**	1.46	6.60	6.54	2.05	2.11
Ba@**1**	1.39	6.57	6.50	2.09	2.15
Ca@**2**	1.21	6.41	6.35	2.14	2.26
Sr@**2**	1.23	6.43	6.37	2.15	2.27
Ba@**2**	1.28	6.43	6.37	2.12	2.28

The triplet-singlet splitting energies ($E_{T\text{-}S}$), vertical ionization energies (E_{VI}), adiabatic ionization energies (E_{AI}), vertical electron affinities (E_{VA}), and adiabatic electron affinities (E_{AA}) of M@**1** and M@**2** were calculated and are listed in Tab.3. Compared with the reported $E_{T\text{-}S}$ of M@C_1(17459)-C_{76}(0.82 eV～0.87 eV) calculated using the same functional, the $E_{T\text{-}S}$ of the two C_{66} based EMMFs are considerably larger, which further validates their higher kinetic stabilities. The M@**1** always have larger $E_{T\text{-}S}$ than the M@**2**, with Ca@**1** having the largest $E_{T\text{-}S}$(1.49 eV) among the six EMFs under study. The E_{VI}'s of M@**1** (6.57 eV～6.60 eV) are always larger than those of M@**2** (6.41 eV～6.43 eV), which means that the M@**1** lose electrons with more difficulty than the M@**2**. The E_{VA}'s of M@**2** (2.12 eV～2.15 eV) are always larger than those of M@**1** (2.01 eV～2.09 eV), indicating that the M@**2** accept electrons more easily. Clearly, for a given cage, there is little change (below 0.08eV) in these energies as the encapsulated metal changes from Ca to Ba. Moreover, from the differences between vertical energies and adiabatic energies, one notes that the reorganization

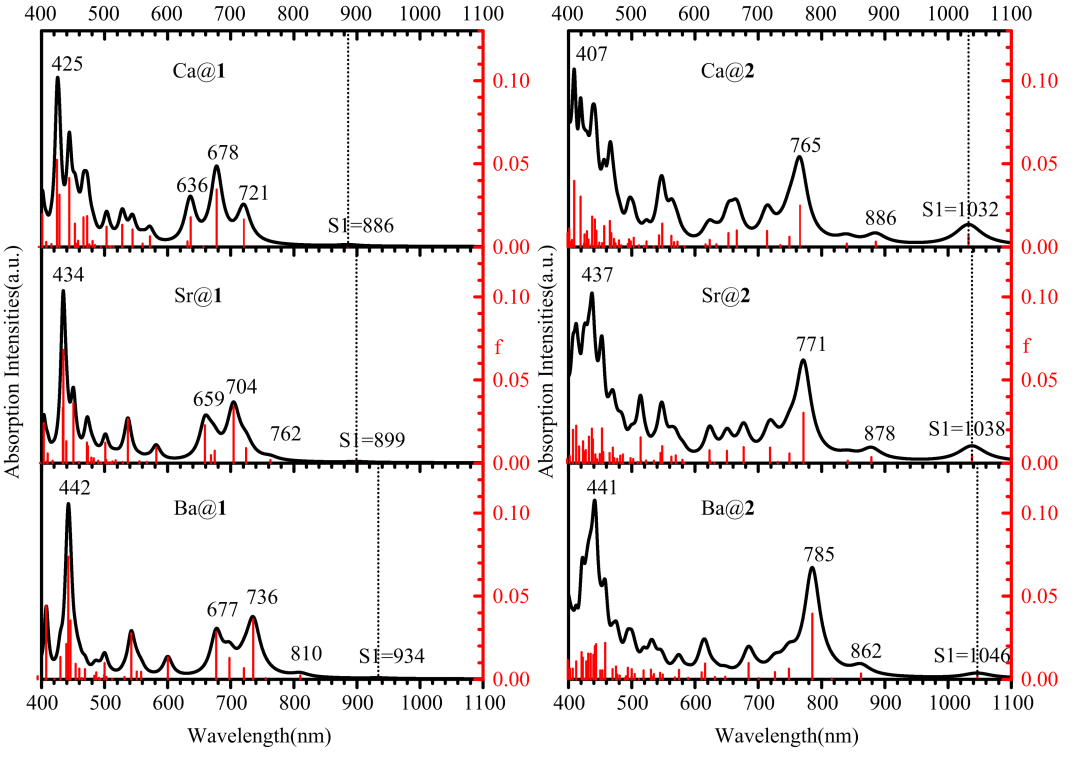

Fig. 4 Simulated Vis-NIR spectra of M@ C_{2v}(4348)-C_{66}(M@**1**) and M@ C_2(4466)-C_{66}(M@**2**)(M = Ca, Sr, Ba), transition oscillator strengths (f) are indicated by red-colored bars (scaled by the right *y*-axis), and positions of transitions to the first excited states (S1) are indicated by dotted lines. Spectral lines were broadened using Gaussian functions with full width at half maximum being 0.06 eV.

energies are quite small (about 0.06 eV) during the process of losing or accepting electrons, suggesting that these compounds might have potential application as photovoltaic materials, as is the case of the well-known I_h-C_{60} and other EMFs.

3.3 Spectra of M@C_{2v}(4348)-C_{66} and M@C_2(4466)-C_{66}

In this section we provide simulated Vis-NIR, IR, Raman and ^{13}C NMR spectra of M@**1** and M@**2**. The differences between the two series of M@C_{66} are emphasized, which should be helpful for characterizing compounds in future experiments.

Vis-NIR spectra are very important characterization tools for EMFs. They can be used to identify which fullerene structure is adopted by an unknown EMF in combination with previously measured spectra or theoretical calculations. Simulated Vis-NIR spectra of M@**1** and M@**2** are displayed in Fig. 4. Just as for other fullerenes and EMFs, absorption intensities in the visible and near-IR region in the range 400 nm～1100 nm of the two series of M@C_{66} are rather weak, due to their relatively small transition dipole moments (f indicated by the right *y*-axes in Fig. 4) between the ground state and low-lying excited states. The wavelengths at which prominent peaks occur are marked by numbers in Fig. 4 and positions of transitions to the first excited states (S1) are indicated by dashed lines. It should be noted that transitions to the S1s of M@**1** are not symmetry-forbidden but possess a small transition dipole moment nevertheless. They still should be observable in experimental spectra given the possibility of vibronic coupling. The S1 transitions are at 886 nm, 899 nm, and 934 nm for Ca@**1**, Sr@**1** and Ba@**1**, respectively, with a red shift being observed as the metal changes from Ca to Ba. Electronic transitions from HOMO to LUMO make dominant contributions to excitations to S1s for M@**1**, so changes to the excited state energies of the S1's are consistent with changes in the HOMO-LUMO gaps in Tab.1 as the encapsulated metal changes. For Ca@**2**, Sr@**2** and Ba@**2**, transitions to the S1s occur at 1032 nm, 1038 nm and 1046 nm, respectively, with relatively stronger intensities and at longer wavelengths compared to the corresponding M@**1** compounds. Red shifts also occur for transitions to the S1s of M@**2** as M changes from Ca to Ba, but the HOMO-LUMO gaps became a little larger, as can be seen in Tab.1. This divergence is induced by the fact that there are comparable contributions to the transition state energies from HOMO to LUMO+2 in S1, in addition to the major HOMO to LUMO contribution. Actually, the extent of this M@**2** red shift is rather small compared with that of M@**1**. There are four distinct peaks for Ca@**1** at 425 nm, 636 nm, 678 nm and 721 nm, with the peaks between 425 nm and 636 nm possibly fusing to form one

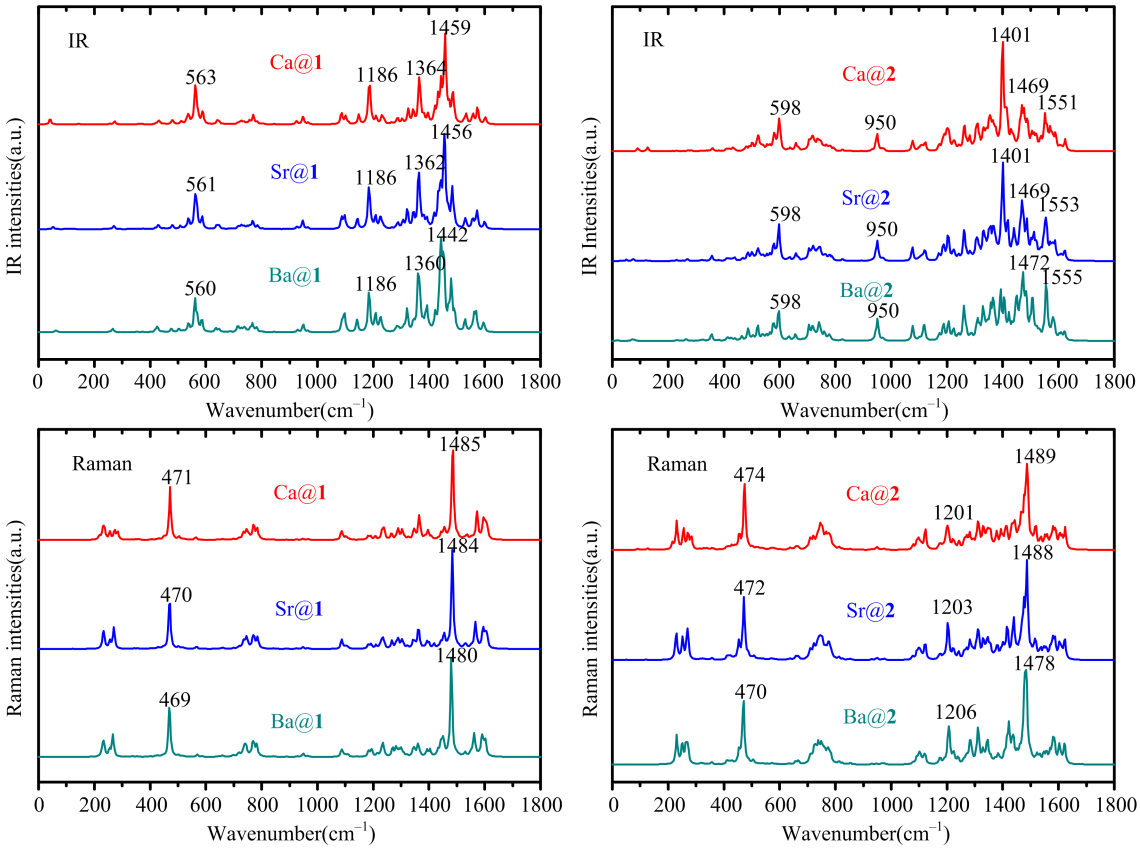

Fig. 5 Simulated IR and Raman spectra of M@C_{2v}(4348)-C_{66}(M@**1**) and M@C_2(4466)-C_{66}(M@**2**) (M=Ca, Sr, Ba).

or more broad bands. The peaks for Sr@**1** at 434 nm, 537 nm, 659 nm as well as at 704 nm, and the peaks for Ba@**1** at 442 nm, 542 nm, 677 nm and 736 nm are easily observed in experimental spectra. For M@**2**, distinct, relatively strong absorption peaks occurring at 765 nm for Ca, 771 nm for Sr and 785 nm for Ba are easily discernable, with a red shift of 20 nm as M changes from Ca to Ba.

Vibrational spectroscopy is quite useful for the experimental characterization of EMFs. Thus IR and Raman spectra of the two series of M@C_{66}'s were simulated and displayed in Fig. 5. Obviously, spectra of M@**1** always have fewer peaks than M@**2** compounds, because the symmetry of M@**1** (C_{2v}) is higher than that of M@**2** (C_1). In the IR spectra of M@**1** compounds there is a distinct peak at about 561 cm^{-1} for M@**1** and at about 598 cm^{-1} for M@**2**, respectively. There is a narrow peak at 950 cm^{-1} and a relatively broad band between 700 cm^{-1} and 800 cm^{-1} in the IR spectrum of M@**2**, while absorptions at similar positions in the IR of M@**1** are rather weak. The strongest absorptions for M@**1** were at 1459 cm^{-1}, 1456 cm^{-1} and 1442 cm^{-1} for M=Ca, Sr or Ba, respectively. There were two distinct peaks at 1186 cm^{-1} and 1364 cm^{-1} for Ca@**1**. The position of the former peak remains fixed as M changes to Sr and Ba, while the latter has a slight red shift. The strongest peaks for Ca@**2** and Sr@**2** are located at the same 1401 cm^{-1} position, accompanied by peaks at 1469 cm^{-1} and 1551 cm^{-1} for Ca@**2** as well as at 1469 cm^{-1} and 1553 cm^{-1} for Sr@**2**. For Ba@**2**, the strongest peak is at 1472 cm^{-1}, followed by a distinct peak at 1555 cm^{-1}. The Raman spectra for M@**1** and M@**2** are similar. Both sets of compounds have strong and sharp absorption bands at around 1480 cm^{-1}, a distinct peak at around 470 cm^{-1} and two small absorption bands at around 200 cm^{-1} ~ 300 cm^{-1} and 700 cm^{-1} ~ 800 cm^{-1}. The vibrational mode for the relative motion between the encapsulated metal and outside cage has little Raman intensity when M is Ca, located at 218 cm^{-1} for Ca@**1** and at 215 cm^{-1} for Ca@**2**. But it is hard to distinguish it from the other low-frequency modes of the carbon cage near that frequency.

The ^{13}C NMR spectrum is also an often used experimental tool to characterize EMFs. Symmetry information about the fullerene cage can be easily revealed by checking the number and intensity of ^{13}C NMR signals. Here we simulated the ^{13}C NMR spectra of the two kinds of EMFs by using the GIAO method. The calculated ^{13}C chemical shielding tensors were calibrated to the experimentally observed highest-field

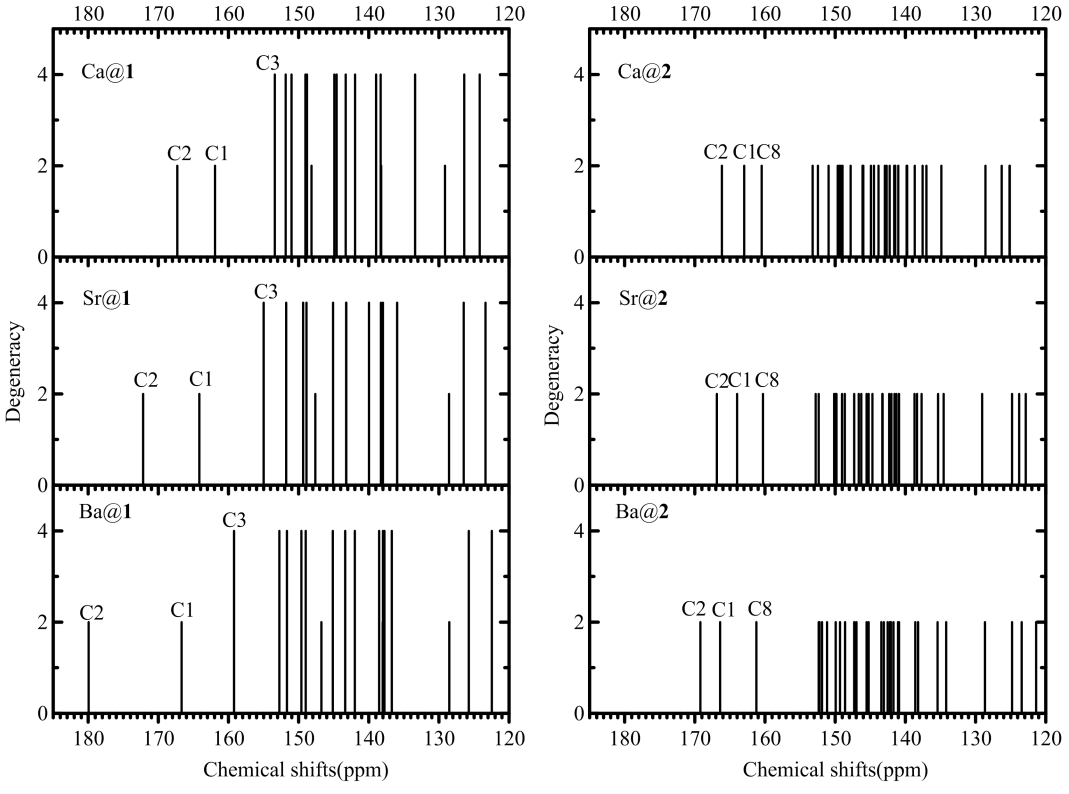

Fig. 6 Simulated ^{13}C NMR spectra of M@C_{2v}(4348)-C_{66}(M@**1**) and M@C_2(4466)-C_{66}(M@**2**)(M=Ca, Sr, Ba).

line of Sc_2@C_{66} at 167.9 ppm [7]. Especially for M@**2**, the influence of the encapsulated metal was averaged because it is likely to hop quickly between the two sites in the cage at the room temperature, just as it does in Ca@D_{3h}-C_{74} and other EMFs. As shown in Fig. 6, a total of 19 peaks can be found in the spectra for M@**1**, including 14 full signals and 5 half signals. For M@**2**, there are 33 signals with the same intensities. One can also see for both series of EMFs, that most peaks distribute densely in the typical sp^2-hybridization range between 120 and 155 ppm, and three distinct peaks are located in the high-field region above 155 ppm. The two highest-field signals belong to the two carbon atoms C2 and C1 (and their equivalent atoms) with [5, 5]-bonds for both M@**1** and M@**2**, just the same as in the case of Sc_2@C_{66}[10]. The carbon atoms (C3/C8/C9/C11 for M@**1** and C8/C48 for M@**2**) adjacent to the [5, 5]-bond also have higher chemical shifts than most other carbon atoms. Identity of the encapsulated metal atom greatly influences the position of the highest-field peak for M@**1**, which moves to higher field as the atomic radius increases from Ca to Ba. For Ca@**1**, the highest-field peak is located at 167.3 ppm, a little lower than the corresponding peak of Sc_2@C_{66}, and it shifts to 172.2 ppm and 179.9 ppm for Sr@**1** and Ba@**1**, respectively.

4 Conclusions

Structures of fullerene C_{66} cages encapsulating an atom of the alkaline earths Ca, Sr and Ba have been investigated by using theoretical calculations. Out of the 137065 C_{66} isomers that could be considered, the non-IPR cage C_{2v}(4348)-C_{66} with two APPs is predicted to be the most likely cage structure for compounds of the type M@C_{66} where M is Ca, Sr or Ba. The proposed M@C_{2v}(4348)-C_{66} structure possesses not only the lowest energy at absolute zero among all the M@C_{66} isomers considered, but also the highest thermodynamic stability at the high temperatures required for the production of EMFs, according to statistical thermodynamic analysis. The two labile APP motifs in the C_{2v}(4348)-C_{66} cage are adjacent, which enables the encapsulated alkaline earth metal to bind to and stabilize both of them at the same time. The resulting local aromaticity and relatively large HOMO-LUMO gaps endow the M@C_{2v}(4348)-C_{66}—especially Ca@C_{2v}(4348)-C_{66}—with high kinetic stabilities, which should facilitate their isolation from arc-discharge carbon soot. Besides C_{2v}(4348)-C_{66}, another cage—C_2(4466)-C_{66}— may also be found because of its large predicted abundance at high temperatures when Sr or Ba is encapsulated. But the local aromaticity of the latter cage is not as high as that of M@C_{2v}(4348)-C_{66}, which may make its extraction difficult. Simulated Vis-NIR, IR, Raman and ^{13}C NMR

spectra for both M@C_{2v}(4348)-C_{66} and M@C_2(4466)-C_{66} cages are provided, which should be useful to further the experimental identification and characterization of these compounds.

Supplementary data

Supplementary data are available at J. Univ. Sci. Tech. China online.

Acknowledgements

This work was supported by the National Natural Science Foundation of China (21963004), Plan Project for Guizhou Provincial Science and Technology (QKH-Basic [2018]1022).

Conflict of interest

The authors declare no conflict of interest.

Author information

CUI Peng received his Ph.D. degree in Theoretical and Computational Chemistry from Shandong University, China. He is currently an associate professor at Guizhou University of Finance and Economics. His research interests cover fullerene-based electronic devices, and high-performance computations, and machine learning.

JIANG Jun (corresponding author) received his Ph.D. degree in Theoretical Chemistry at Royal Institute of Technology, Sweden. He is currently a professor at University of Science and Technology of China. His major research interests focus on the development and employment of multi-scale modeling methods for exciton kinetics in complex system, while targeting on a wide range of physics and chemistry applications such as photocatalysis, photochemistry, and nonlinear spectroscopy.

References

[1] Popov A A, Yang S, Dunsch L. Endohedral fullerenes. Chem. Rev., 2013, 113: 5989-6113.

[2] Lu X, Feng L, Akasaka T, et al. Current status and future developments of endohedral metallofullerenes. Chem. Soc. Rev., 2012, 41: 7723-7760.

[3] Rodriguez-Fortea A, Balch A L, Poblet J M. Endohedral metallofullerenes: a unique host-guest association. Chem. Soc. Rev., 2011, 40: 3551-3563.

[4] Chai Y, Guo T, Jin C, et al. Fullerenes with metals inside. J. Phys. Chem., 1991, 95: 7564-7568.

[5] Reich A, Panthofer M, Modrow H, et al. The structure of Ba@C_{74}. J. Am. Chem. Soc., 2004, 126: 14428-14434.

[6] Che Y, Yang H, Wang Z, et al. Isolation and structural characterization of two very large, and largely empty, endohedral fullerenes: Tm@C_{3v}-C_{94} and Ca@C_{3v}-C_{94}. Inorg. Chem., 2009, 48: 6004-6010.

[7] Wang C R, Kai T, Tomiyama T, et al. C_{66} fullerene encaging a scandium dimer. Nature, 2000, 408: 426-427.

[8] Kobayashi K, Nagase S. A stable unconventional structure of Sc_2 @ C_{66} found by density functional calculations. Chem. Phys. Lett., 2002, 362: 373-379.

[9] Takata M, Nishibori E, Sakata M, et al. Sc_2 dimer in IPR-violated C_{66} fullerene: a covalent bonded metallofullerene. Chem. Phys. Lett., 2003, 372: 512-518.

[10] Yamada M, Kurihara H, Suzuki M, et al. Sc_2@C_{66} revisited: an endohedral fullerene with scandium ions nestled within two unsaturated linear triquinanes. J. Am. Chem. Soc., 2014, 136: 7611-7614.

[11] Tan Y Z, Li J, Zhu F, et al. Chlorofullerenes featuring triple sequentially fused pentagons. Nat. Chem., 2010, 2: 269-273.

[12] Gao C L, Li X, Tan Y Z, et al. Synthesis of long-sought C_{66} with exohedral stabilization. Angew. Chem. Int. Ed., 2014, 53: 7853-7855.

[13] Tian H R, Chen M M, Wang K, et al. An unconventional hydrofullerene $C_{66}H_4$ with symmetric heptagons retrieved in low-pressure combustion. J. Am. Chem. Soc., 2019, 141: 6651-6657.

[14] Li Q Z, Zheng J J, He L, et al. Stabilization of a chlorinated # 4348 C_{66}: C_{2v} cage by encapsulating monometal species: coordination between metal and double hexagon-condensed pentalenes. Inorg. Chem., 2016, 55: 7667-7675.

[15] Bao X, Kong X. Generation of M@C_{2n+} (M=Ca, Sr, Ba, 2n=50—230) by laser ablation of graphene. Int. J. Mass. Spectrom., 2014, 372: 1-7.

[16] Cui Y H, Tian W, Feng J K, et al. Structures, stabilities, aromaticity, and electronic properties of C66 fullerene isomers, anions ($C66^{2-}$, $C66^{4}$, $C66^{6}$), and metallofullerenes (Sc_2@C_{66}). J. Nanopart. Res., 2010, 12: 429-438.

[17] Zhao R, Guo Y, Zhao P, et al. Warning to theoretical structure elucidation of endohedral metallofullerenes. J. Phys. Chem. C, 2016, 120: 1275-1283.

[18] Schleyer P V R, Maerker C, Dransfeld A, et al. Nucleus-independent chemical shifts: a simple and efficient aromaticity probe. J. Am. Chem. Soc., 1996, 118: 6317-6318.

[19] Wolinski K, Hinton J F, Pulay P. Efficient implementation of the gauge-independent atomic orbital method for NMR chemical shift calculations. J. Am. Chem. Soc., 1990, 112: 8251-8260.

[20] Chen N, Beavers C M, Mulet-Gas M, et al. Sc_2S@C_s(10528)-C_{72}: a dimetallic sulfide endohedral fullerene with a non isolated pentagon rule cage. J. Am. Chem. Soc., 2012, 134: 7851-7860.

[21] Frisch M J, Trucks G W, Schlegel H B, et al. Gaussian 09. Wallingford, CT, USA: Gaussian, Inc., 2009.

[22] Brinkmann G, Delgado Friedrichs O, Lisken S, et al. CaGe - a virtual environment for studying some special classes of plane graphs - an update. MATCH Commun. Math. Comput. Chem., 2010, 63: 533-552.

[23] Humphrey W, Dalke A, Schulten K. VMD: Visual molecular dynamics. J. Mol. Graph., 1996, 14: 33-38.

[24] Gan L H, Zhao J Q, Hui Q. Nonclassical fullerenes with a heptagon violating the pentagon adjacency penalty rule. J. Comput. Chem., 2010, 31: 1715-1721.

[25] Stone A J, Wales D J. Theoretical studies of icosahedral C_{60} and some related species. Chem. Phys. Lett., 1986, 128: 501-503.

[26] Diener M D, Alford J M. Isolation and properties of small-bandgap fullerenes. Nature, 1998, 393: 668-671.

[27] Dennis T J S, Shinohara H. Production and isolation of the C_{80}-based group 2 incar-fullerenes: $iCaC_{80}$, $iSrC_{80}$ and $iBaC_{80}$ [J]. Chem. Commun., 1998, 883-884.

[28] Cui J B, Guo Y J, Li Q Z, et al. Theoretical survey on M@C_{80} (M=Ca, Sr, and Ba): Behavior of different alkaline earth metal impacting the chemical stability and electronic

properties. Chem. Phys., 2016, 474: 7-17.
[29] Yang T, Zhao X, Xu Q, et al. Probing the role of encapsulated alkaline earth metal atoms in endohedral metallofullerenes M@C_{76}(M = Ca, Sr, and Ba) by first-principles calculations. Dalton Trans., 2012, 41: 5294-5300.
[30] Schmalz T G, Seitz W A, Klein D J, et al. Elemental carbon cages. J. Am. Chem. Soc., 1988, 110: 1113-1127.
[31] Tan Y Z, Xie S Y, Huang R B, et al. The stabilization of fused-pentagon fullerene molecules. Nat. Chem., 2009, 1: 450-460.

单金属富勒烯 M@C66（M=Ca，Sr，Ba）结构、稳定性及谱学的第一性原理计算研究

崔鹏[1,2]，张竹霞[3]，Edward SHARMAN[4]，江俊[2*]
1.贵州财经大学信息学院，贵州贵阳 550025；2.中国科学技术大学化学与材料科学学院，安徽合肥 230026；
3.太原理工大学航空航天学院，山西太原 030024；
4. 加州大学欧文分校神经学系，加利福尼亚州尔湾市 92697，美国

摘要：由于产量非常低，许多内嵌金属富勒烯（EMF）的结构尚不清楚，特别是碳笼碳数在 70 以下的单金属富勒烯.通过密度泛函理论（DFT）对内嵌碱土金属的单金属富勒烯 M@C_{66}（M=Ca，Sr 和 Ba）进行了理论计算研究.能量计算和统计热力学分析表明，在所考虑的众多 C_{66} 富勒烯异构体中，内嵌 Ca、Sr 和 Ba 后，碳笼 C_{2v}(4348)-C_{66} 能量最低，但在高温情况下，另外一种碳笼 C_2(4466)-C_{66} 也有较高的分布.这两类金属富勒烯 M@C_{2v}(4348)-C_{66} 和 M@C_2(4466)-C_{66} 的 HOMO-LUMO 间隙较大，且都具有较强的局部芳香性，可能在将来的实验中被发现.此外，还计算了这两类金属富勒烯的近红外可见光吸收谱、红外谱、拉曼谱以及 ^{13}C 核磁共振谱，以协助将来的实验表征.

关键词：金属富勒烯；并五元环；理论计算